Interferometric mass photometry at the quantum limit of sensitivity

Fabian Müller,[1] Emre Köse,[1] Alfred J. Meixner,[2] Erik Schäffer,[3] and Daniel Braun[1]
[1]*Institut für Theoretische Physik, Eberhard Karls Universität Tübingen, 72076 Tübingen, Germany*
[2]*Institut für Physikalische und Theoretische Chemie, Eberhard Karls Universität Tübingen, 72076 Tübingen, Germany*
[3]*Cellular Nanoscience (ZMBP), Eberhard Karls Universität Tübingen, 72076 Tübingen, Germany*

(Received 8 November 2024; accepted 3 March 2025; published 1 April 2025)

We present an innovative optical imaging system for measuring parameters of a small particle such as a macromolecule or nanoparticle at the quantum limit of sensitivity. In comparison to the conventional confocal interferometric scattering (iSCAT) approach, our setup adds a second arm to form a Michelson interferometer that allows us to tune a relative phase. We evaluate the quantum Cramér-Rao bound (QCRB) for different quantum states, including single-mode coherent states, multifrequency coherent states, and phase-averaged coherent states. Our results show that the proposed setup can achieve the QCRB of sensitivity and outperform iSCAT for all considered quantum states for the mass and phase estimation of a particle.

DOI: 10.1103/PhysRevA.111.043501

I. INTRODUCTION

Recent advancements in optical imaging have significantly improved the estimation of the parameters of the targeted system and widened applications across fields such as physics, biology, and medicine [1–11]. Despite the remarkable progress in classical imaging technologies, even the most advanced conventional microscopes have not yet reached the optimal quantum limit of resolution set by the quantum Cramér-Rao bound (QCRB), which in the context of imaging is the best resolution optimized over all possible measurements and data analysis schemes [12–16]. It is given by the inverse of the quantum Fisher information (QFI), which in turn sets an upper bound to the classical Fisher information (CFI) from any specific measurement to estimate a specific parameter. Achieving the QCRB would require overcoming all technical problems, such as stability issues of thermal and technical noise, leaving only the fundamental quantum noise present in the quantum state of light. Interferometric imaging plays an important role in mass photometry, where the mass of a small particle, such as a protein molecule, is estimated based on the light it scatters [3,4,13,17–19]. When incident light interacts with a particle it induces a dipole moment leading to Rayleigh scattering [20,21]. The polarizability of the particle is related to its volume and for a spherical particle gives a linear relationship between the mass of the particle and the scattered-field amplitude [22]. Due to the small scattering cross section of individual particles, the estimation of parameters from the particle is challenging. In addition, some light is reflected from the glass surface on which the particle rests. This reflected field carries no information about the parameters of the particle, thereby reducing the CFI derived from the intensity measurements. Dark-field microscopy can eliminate this reflected light and the QCRB can be achieved for mass estimation of the nanoparticle if there is no noise from the detector, which, however, is challenging to achieve. Further, there is no information about the position of the particle or other information carried by the phase [23,24]. In interferometric scattering microscopy (iSCAT), one uses the interference of the scattered light from a nanoparticle and the reflected light from the glass, which also allows phase estimation [1,25–28]. However, in general, iSCAT does not saturate the QCRB for either phase or mass estimation. To address these limitations and understand the fundamental constraints on parameter estimation, we propose a combination of iSCAT with a Michelson interferometer as an alternative and highly flexible setup [Michelson interferometric scattering microscopy (MiSCAT)]. We analyze the QFI and the QCRB for this setup and compare them to confocal iSCAT [29–33]. It becomes clear that optimizing the phase and amplitude of the light in the second arm of the Michelson interferometer is crucial for improving parameter estimation and reaching the quantum limit of sensitivity.

The structure of the paper is as follows. Section II describes the theoretical model for the MiSCAT and provides an analysis of the QCRB for different quantum states, including single-mode coherent states, phase-averaged coherent states, multifrequency-mode coherent states, and phase-averaged multifrequency-mode coherent states. In Sec. III we present the results for the CFI using optimal photon-number measurements and discuss the conditions for achieving the QCRB using MiSCAT for different parameters such as the mass and phase of the nanoparticle. We provide a comparison between MiSCAT and iSCAT, highlighting potential advantages, and the results are supported by an analysis of the signal-to-noise ratio. In Sec. IV we summarize and discuss our results.

II. THEORY

The MiSCAT, shown in Fig. 1(a), is inspired by a nanoscale plasmonic phase sensor recently studied by one of us [31,33]. Here we optimize it for photometry. We denote by E_s and E_r the real amplitudes of the positive-frequency components of the scattered and reflected electric fields, respectively, for a chosen polarization direction. The first arm of the interferometer contains the scattered light $E_s e^{i\phi_s}$ with the parameters imprinted on the quantum state, where ϕ_s is the relative phase

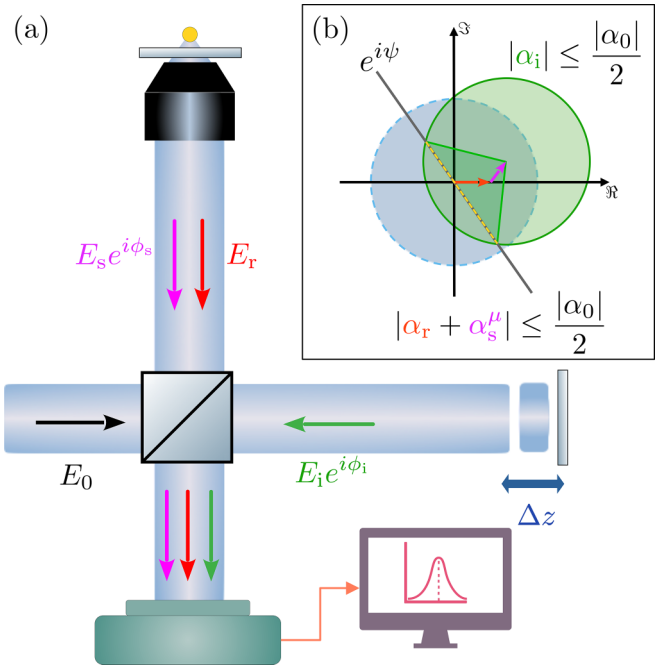

FIG. 1. (a) Setup for MiSCAT mass photometry. A laser source illuminates the sample with an initial incoming field denoted by E_0. The light scattered by the particle from the sample is represented by the field $E_s e^{i\phi_s}$. A first glass plate reflects a portion of the incoming field, denoted by E_r. To achieve optimal sensitivity, a phase in the total field adjusted by a second interferometric arm introduces a precisely controlled $E_i e^{i\phi_i}$. This additional field is carefully adjusted and ensures that the total field $E_r + E_s e^{i\phi_s} + E_i e^{i\phi_i}$ arriving at the single-point detector gives a specific phase, enabling us to achieve the quantum limit of sensitivity. (b) Corresponding coherent-state labels in the complex plane. The yellow dashed line shows the solution space of α_i to saturate the QCRB of mass estimation.

of the scattered light with respect to the reflected light, and the reflected light E_r from the glass interface of the sample holder, corresponding to a typical iSCAT configuration [4]. The reference arm (second arm) is used to optimize the total field which includes the imprinted parameter. Thus, we consider the reference arm as adjustable in its length and reflectivity. The adjustable reflectivity allows one to tune the amplitude E_i, while the change of the length of the arm results in a relative phase $\phi_i = 2k\Delta z$ compared to the reflected field of the first arm. This yields a positive-frequency component of the electric field with fixed polarization direction from the reference arm as $E_i e^{i\phi_i}$. Before the detection, a beam splitter superposes the fields from both arms, yielding $E_d = E_r + E_s e^{i\phi_s} + E_i e^{i\phi_i}$ as the positive-frequency component of the total field at the detector [32,33]. We can now investigate the information contained in the scattered light in different kinds of states. We first consider the single-mode states and then multifrequency-mode states.

Quantum Cramér-Rao bound

1. Single-mode coherent state

We consider a single-mode coherent state $\rho^0 = |\alpha_0\rangle\langle\alpha_0|$ as an initial quantum state produced by a laser source with initial average photon number $\bar{n}^0 = |\alpha_0|^2$, which translates the positive-frequency component of the electric field to labels of the coherent states [34]. We neglect any nonlinear and dissipative effects such that an incoming coherent state propagates to a coherent state of the field at the detector. The 50:50 beam splitter (BS) acts as a unitary transformation on two incoming modes. The action of the beam splitter and the arms on the initial field is

$$(\alpha_0, 0) \xrightarrow{\text{BS}} \left(\frac{\alpha_0}{\sqrt{2}}, \frac{\alpha_0}{\sqrt{2}}\right) \xrightarrow{\text{reflection}} \left(\tilde{\alpha}_r + \tilde{\alpha}_s^\mu, \tilde{\alpha}_i\right), \tag{1}$$

under the assumption that no field is reflected from the detector, where the first term corresponds to the reflected field in the first arm including the reflection from the glass interface $\tilde{\alpha}_r$ and scattering from the nanoparticle $\tilde{\alpha}_s^\mu$, with the superscript μ the parameter to be estimated, carried by the complex label $\tilde{\alpha}_s^\mu$, and the second term is the reflected field from the reference arm $\tilde{\alpha}_i$. Both fields pass again through the beam splitter and the coherent-state labels become

$$\left(\tilde{\alpha}_r + \tilde{\alpha}_s^\mu, \tilde{\alpha}_i\right) \xrightarrow{\text{BS}} \left(\frac{\tilde{\alpha}_r + \tilde{\alpha}_s^\mu - \tilde{\alpha}_i}{\sqrt{2}}, \frac{\tilde{\alpha}_r + \tilde{\alpha}_s^\mu + \tilde{\alpha}_i}{\sqrt{2}}\right), \tag{2}$$

with the redefined amplitudes $\alpha_{r,s,i} := \frac{\tilde{\alpha}_{r,s,i}}{\sqrt{2}}$. As there is no additional photon source in the setup, before the recombination of the two arms by the beam splitter, it holds that $|\alpha_r + \alpha_s^\mu| \leqslant \frac{|\alpha_0|}{2}$ and $|\alpha_i| \leqslant \frac{|\alpha_0|}{2}$. The state of light at the detector becomes

$$|\alpha_0\rangle \xrightarrow{\text{setup}} |\alpha_d\rangle = \left|\alpha_r + \alpha_s^\mu + \alpha_i\right\rangle, \tag{3}$$

corresponding to the second term in Eq. (2), while the first term is not accessible.

The complex labels α_r and α_i represent the fields from different arms of the interferometer. In general, the electric field contains both polarization directions in the detection plane. For simplicity, we ignore the second polarization of the field for the coherent state. For a roughly spherical biomolecule with radius much smaller than the wavelength, we have a linear parameter dependence of the label of the coherent state $\alpha_s^\mu = mse^{i\phi_s}$ on the mass m, where ϕ_s is the phase of the light scattered from the particle and s is a real proportionality factor with dimension of inverse mass. The interesting parameters for this setup are either the mass m or phase ϕ_s of the scattered light, $\mu \in \{m, \phi_s\}$. Since there are no additional photons created in the setup, coherent-state labels are constraint by the relation $|\alpha_d|^2 \leqslant |\alpha_0|^2$. This yields an upper bound on each arm, $|\alpha_r + \alpha_s^\mu| \leqslant |\alpha_0|/2$ and $|\alpha_i| \leqslant |\alpha_0|/2$. The factor $1/2$ arises from the transformation of the 50:50 beam splitter. The QCRB gives the minimum standard deviation of any local unbiased estimator $\tilde{\mu}$ of the parameter μ to be estimated. For a single parameter, the bound of the unbiased estimator reads

$$\delta\tilde{\mu} \geqslant \sqrt{\frac{1}{\mathcal{F}^\mu}}, \quad \mathcal{F}^\mu = \mathrm{Tr}\left(\rho \mathcal{L}_\mu^2\right), \tag{4}$$

where $\mathcal{F}^\mu$ is the QFI of the parameter μ and $\mathcal{L}_\mu$ is the symmetric logarithmic derivative (SLD), defined by $\partial_\mu \rho = \frac{1}{2}(\mathcal{L}\rho + \rho\mathcal{L})$ [12,16]. The QFI for the parameter μ in the coherent state $\rho_c^d = |\alpha_d\rangle\langle\alpha_d|$ with subscript c is given by the partial derivative of α_s^μ with respect to the parameter μ as $\mathcal{F}_c^\mu = 4|\partial_\mu \alpha_s^\mu|^2$ and it is completely independent of α_i and α_r (see Appendix A). However, we will show later that in general

there is no measurement that can achieve the QCRB if we have α_r without the reference arm. Due to the linear parameter dependence on m, its QFI becomes independent of m and of ϕ_s [24]. Regarding the number of scattered photons from the particle, $\bar{n}_c^s = |\alpha_s^\mu|^2$, one obtains the relative uncertainty from the QCRB bound for mass estimation as

$$\frac{\delta m}{m}\sqrt{\bar{n}_c^s} \geqslant \frac{1}{2}. \tag{5}$$

For instance, in [4] the number of scattered photons considering a laser with an intensity $I_0 = 0.1$ MW/cm^2 with wavelength $\lambda = 445$ nm and effective exposure time $\Delta t = 100$ ms from a biomolecule with a mass of 66 kDa and a radius 3.8 nm was found to be $\bar{n}_c^s \approx 220$, which leads to $s \simeq 0.22$ kDa^{-1}. Using this value, the relative uncertainty in the quantum limit for mass estimation is $\delta m \approx 2$ kDa, or, keeping the exposure time more general, $(\delta m)^2 \Delta t \approx 0.5$ (kDa)^2/Hz for the 66 kDa protein.

2. *Phase-averaged coherent states*

The coherent states have definite phase. However, a more realistic model of the electric field produced by a laser contains a randomly fluctuating phase that can be modeled as a mixture of coherent states with uniformly distributed phase $\rho_p^0 = \int_0^{2\pi} d\gamma_0 |\alpha_0 e^{i\gamma_0}\rangle\langle\alpha_0 e^{i\gamma_0}|/2\pi$, where α_0 is a real amplitude and γ_0 is the corresponding phase that is averaged [35,36]. In the detector, we have

$$\rho_p^d = \frac{1}{2\pi}\int_0^{2\pi} d\gamma_0 |\alpha_d e^{i\gamma_0}\rangle\langle\alpha_d e^{i\gamma_0}|, \tag{6}$$

where $\alpha_d = \alpha_r + \alpha_s^\mu + \alpha_i$ and the subscript p stands for the phase-averaged coherent state. Expanding ρ_p^d in the Fock basis and carrying out the integral using $\int_0^{2\pi} d\phi\, e^{i\phi(n-m)} = 2\pi\delta_{nm}$, we obtain the state as

$$\begin{aligned}\rho_p^d &= \sum_{n,m}\int_0^{2\pi}\frac{d\gamma_0}{2\pi} e^{-|\alpha_d|^2}\frac{(\alpha_d^n)(\alpha_d^m)^* e^{i\gamma_0(n-m)}}{(n!)^{1/2}(m!)^{1/2}}|n\rangle\langle m| \\ &= \sum_n e^{-|\alpha_d|^2}\frac{|\alpha_d|^{2n}}{n!}|n\rangle\langle n| = \sum_n P_n|n\rangle\langle n|,\end{aligned} \tag{7}$$

with Poisson's distribution P_n. The SLD of this state is directly obtained from it as

$$\begin{aligned}\mathscr{L}_p &= \sum_n \frac{\partial_\mu P_n}{P_n}|n\rangle\langle n| \\ &= -2\,\mathrm{Re}(\alpha_d^*\partial_\mu\alpha_d)\sum_n\left(1-\frac{n}{|\alpha_d|^2}\right)|n\rangle\langle n|.\end{aligned} \tag{8}$$

In the second step, we used that the derivative of the Poisson distribution is

$$\partial_\mu P_n = -2\,\mathrm{Re}(\alpha_d^*\partial_\mu\alpha_d)\left(1-\frac{n}{|\alpha_d|^2}\right)P_n. \tag{9}$$

The QFI then becomes

$$\begin{aligned}\mathscr{F}_p^\mu &= 4\,\mathrm{Re}^2(\alpha_d^*\partial_\mu\alpha_d)\sum_n\left(1-\frac{n}{|\alpha_d|^2}\right)^2 P_n \\ &= 4\,\mathrm{Re}^2(\alpha_d^*\partial_\mu\alpha_d)\left(1-2\frac{\langle n\rangle}{|\alpha_d|^2}+\frac{\langle n^2\rangle}{|\alpha_d|^4}\right).\end{aligned} \tag{10}$$

The expectation values occurring in this equation of the QFI are $\langle n\rangle = |\alpha_d|^2$ and $\langle n^2\rangle = |\alpha_d|^4 + |\alpha_d|^2$ for a Poisson distribution. Inserting them into the QFI yields

$$\mathscr{F}_p^\mu = 4\,\mathrm{Re}^2\left(\frac{\alpha_d^*}{|\alpha_d|}\partial_\mu\alpha_s^\mu\right), \tag{11}$$

as only α_s^μ in α_d depends on the parameter. The polar representation of the coherent-state labels $\alpha_d = |\alpha_d|e^{i\chi}$ and its derivative $\partial_\mu\alpha_s^\mu = |\partial_\mu\alpha_s^\mu|e^{i\psi}$ simplifies the QFI to

$$\begin{aligned}\mathscr{F}_p^\mu &= 4\left|\partial_\mu\alpha_s^\mu\right|^2\mathrm{Re}^2(e^{i(\psi-\chi)}) \\ &= 4\left|\partial_\mu\alpha_s^\mu\right|^2\cos^2(\psi-\chi).\end{aligned} \tag{12}$$

Since $\cos^2(\psi-\chi) \leqslant 1$, we see that it is upper bounded by the QFI of the coherent state $\mathscr{F}_p^\mu \leqslant \mathscr{F}_c^\mu$. Clearly, to estimate a parameter in this phase-averaged coherent state, we can first optimize the corresponding phases to reach the QFI of the coherent state. For the parameter m carried by the field amplitude α_s, the QCRB of the relative mass uncertainty becomes

$$\frac{\delta m}{m}\sqrt{\bar{n}_c^s} \geqslant \frac{1}{2|\cos(\psi-\chi)|}. \tag{13}$$

This uncertainty implies that it is optimal if the phase χ of the total field matches the phase ψ of its derivative. The relation between the field from the first arm and the reference arm of the interferometer is shown in Fig. 1(b), where the coherent-state labels are plotted in the complex plain. The blue circle (dashed line) contains all possible coherent-state labels $\alpha_r + \alpha_s^\mu$ of the first arm. The coherent-state label α_i of the reference arm is added to the label of the first arm. Thus all possible coherent states with labels α_d are located in a circle, centered at the coherent-state label of the first arm, which is shown in Fig. 1(b) as a green circle (solid line). The superposition yields the total coherent-state label at the detector $\alpha_d(\mu;\alpha_i,\phi_i)$ as a function of the reference arm's parameters, therefore affecting its phase $\chi(\alpha_i,\phi_i)$. The coherent-state label must have the phase ψ, which corresponds to all labels on the straight line through the origin. All coherent states with labels in the intersection of this line and the green circle, indicated by the yellow dashed line, saturate the QCRB. In general, there is no unique solution but a continuous set of parameters $(|\alpha_i|,\phi_i)$, saturating the QCRB. The contributions of both arms are bounded by $|\alpha_0|/2$ such that the maximum distance of the first arm's coherent-state label $\alpha_r + \alpha_s^\mu$ to the solution space is $|\alpha_0|/2$ and further that there is always a solution satisfying the condition $\psi = \chi$.

3. *Multifrequency-mode coherent states*

Apart from the coherent light, in mass photometry, narrow-bandwidth white light is considered to avoid speckle effects due to laser light [30]. In the following, we take the initial

state of the field produced, for example, by a superluminescent LED [37] as $\rho_0^{\mathrm{f}} = |\{\alpha_0(\omega)\}\rangle\langle\{\alpha_0(\omega)\}|$, labeled by a set of coherent-state amplitudes $\{\alpha_0(\omega)\}$ [34]. The coherent-state labels for this state have SI unit $\mathrm{Hz}^{-1/2}$. We assume that for white light $\alpha_0(\omega) \propto \sqrt{1/\omega}$ (flat intensity distribution) in the bandwidth $\Delta\omega$ of interest. Furthermore, we assume that scattering from the particle does not create any correlations between different frequencies. The resulting state at the detector is then given by $\rho_{\mathrm{f}}^{\mathrm{d}} = |\{\alpha_{\mathrm{d}}(\omega)\}\rangle\langle\{\alpha_{\mathrm{d}}(\omega)\}|$, where $\alpha_{\mathrm{d}}(\omega) = \alpha_{\mathrm{r}}(\omega) + \alpha_{\mathrm{s}}^{\mu}(\omega) + \alpha_{\mathrm{i}}(\omega)$ with additional frequency dependence. Since there are no correlations between different modes, we have a continuous product of coherent states and the QFI becomes $\mathscr{F}_{\mathrm{f}}^{\mu} = 4\int_{\Delta\omega} d\omega |\partial_\mu \alpha_{\mathrm{s}}^{\mu}(\omega)|^2$. For a linear dependence on the mass of the scattered field [4,24] $\alpha_{\mathrm{s}}^{\mu}(\omega) = ms(\omega)e^{i\phi_{\mathrm{s}}(\omega)}$, we find the lower bound on the relative uncertainty of mass estimation $(\delta m/m)\sqrt{\bar{n}_{\mathrm{f}}^{\mathrm{s}}} \geqslant 1/2$, just as for a single-mode coherent state. The scattered photon number from the particle is given by $\bar{n}_{\mathrm{f}}^{\mathrm{s}} = \int_{\Delta\omega} d\omega |\alpha_{\mathrm{s}}^{\mu}(\omega)|^2$. If $\bar{n}_{\mathrm{f}}^{\mathrm{s}} = \bar{n}_{\mathrm{c}}^{\mathrm{s}}$, we obtain the same minimal uncertainty for the estimation of the mass as for the single-frequency light, $(\delta m)_{\mathrm{c}} = (\delta m)_{\mathrm{f}}$. However, with multifrequency light with a flat distribution over frequencies, typically a total photon number can be achieved much higher than with a single mode, $\bar{n}_{\mathrm{f}}^{\mathrm{s}} \gg \bar{n}_{\mathrm{c}}^{\mathrm{s}}$, which results in much smaller minimal uncertainty for the same sample size, $(\delta m)_{\mathrm{f}} \ll (\delta m)_{\mathrm{c}}$.

4. Phase-averaged multifrequency

Furthermore, we consider a phase-averaged multifrequency initial state, where all frequencies are phase averaged independently with the continuous tensor product over frequencies with a bandwidth $\Delta\omega$. Then the state of the light at the detector becomes

$$\rho_{\mathrm{pf}}^{\mathrm{d}} = \bigotimes_{\omega} \int_0^{2\pi} \frac{d\gamma_0(\omega)}{2\pi} |\alpha_{\mathrm{d}}(\omega)e^{i\gamma_0(\omega)}\rangle\langle\alpha_{\mathrm{d}}(\omega)e^{i\gamma_0(\omega)}|, \tag{14}$$

where pf stands for phase-averaged multifrequency coherent state. Assuming no correlations between different frequencies are created by the scattering process, we obtain the QFI as

$$\mathscr{F}_{\mathrm{pf}}^{\mu} = 4\int_{\Delta\omega} d\omega\, \mathrm{Re}^2\left(\frac{\alpha_d^*(\omega)}{|\alpha_{\mathrm{d}}(\omega)|}\partial_\mu \alpha_{\mathrm{s}}^{\mu}(\omega)\right). \tag{15}$$

Introducing the phases $\psi(\omega) = \arg[\partial_\mu \alpha_{\mathrm{s}}^{\mu}(\omega)]$ and $\chi(\omega) = \arg[\alpha_{\mathrm{d}}(\omega)]$ with frequency dependence, we can rewrite the QFI as $\mathscr{F}_{\mathrm{pf}}^{\mu} = 4\int_{\Delta\omega} d\omega |\partial_\mu \alpha_{\mathrm{s}}^{\mu}(\omega)|^2 \cos^2[\psi(\omega) - \chi(\omega)]$. Since $\cos^2[\psi(\omega) - \chi(\omega)] \leqslant 1$ for all ω, the QFI of this state is upper bounded by the QFI of the multifrequency coherent state with the same $\alpha_{\mathrm{d}}(\omega)$ distribution. With the explicit form of $\alpha_{\mathrm{s}}^{\mu}(\omega)$ we find the relative uncertainty in the mass estimation as

$$\frac{\delta m}{m}\sqrt{\bar{n}_{\mathrm{pf}}^{\mathrm{s}}} \geqslant \frac{1}{2}\sqrt{\frac{\int_{\Delta\omega} d\omega |s(\omega)|^2}{\int_{\Delta\omega} d\omega |s(\omega)|^2 \cos^2[\psi(\omega) - \chi(\omega)]}}, \tag{16}$$

where $\bar{n}_{\mathrm{pf}}^{\mathrm{s}} = \int_{\Delta\omega} d\omega |\alpha_{\mathrm{s}}^{\mu}(\omega)|^2$ is the number of scattered photons. This can be optimized and reach the limit of the QFI of the coherent state if for each frequency the phases of the field $\chi(\omega)$ and of its derivative $\psi(\omega)$ match.

III. RESULTS

A. Saturating the QFI for mass estimation

Typical measurement methods in the experiments of iSCAT include cameras or photodiodes, both corresponding to an intensity measurement. The positive-operator-valued measure for the photon-number measurement, which for single-mode coherent states also corresponds to intensity measurement, is given by $\Pi_n = |n\rangle\langle n|$, resulting in a Poisson probability distribution

$$P(n|\mu) = e^{-|\alpha_{\mathrm{d}}|^2}\frac{|\alpha_{\mathrm{d}}|^{2n}}{n!}. \tag{17}$$

Then we obtain the CFI, expressed by noncalligraphic F, as

$$F_{\mathrm{c}}^{\mu} = 4\left|\partial_\mu \alpha_{\mathrm{s}}^{\mu}\right|^2 \cos^2(\chi - \psi). \tag{18}$$

The CFI obtained from a photon-number measurement on a single-mode coherent state is the same as the QFI of phase-averaged coherent states. This equivalence arises because the photon-number measurement does not capture information about the total phase of the light field. Consequently, the CFI from this measurement is equivalent to the QFI of a phase-averaged coherent state. In both cases, achieving the QFI relies heavily on the phase of the reference field. Thus, $\mathscr{F}_{\mathrm{c}}^{\mu}$ is now an upper bound for both the CFI of the coherent state F_{c}^{μ} and the QFI of the phase-averaged state $\mathscr{F}_{\mathrm{p}}^{\mu}$ and $F_{\mathrm{c}}^{\mu} = \mathscr{F}_{\mathrm{p}}^{\mu}$.

In general, the reflected-field intensity from the glass interface is three orders of magnitude smaller than the initial field intensity. Additionally, the intensity of scattered light from the particle is approximately six orders of magnitude smaller than the reflected-field intensity for a typical iSCAT setup for mass estimation [3,4]. In Fig. 2(a) we show $F_{\mathrm{c}}^{m}/\mathscr{F}_{\mathrm{c}}^{m}$ without the reference arm of the interferometer. We fixed the amplitude of the scattered field relative to the initial field as $|\alpha_{\mathrm{s}}^{\mu}| = 2\times 10^{-5}|\alpha_0|$. We see that if there is a reflected field, the CFI for estimating the mass from photon-number measurements always drops as a function of α_{r} in a way depending on ϕ_{s}. The QFI of the coherent state is only saturated for $\alpha_{\mathrm{r}} = 0$, which corresponds to dark-field microscopy. However, there is always a reflected field in an iSCAT setup ($\alpha_{\mathrm{r}} \neq 0$), preventing the saturation of the QFI. Furthermore, the reflected-field amplitude is usually considerably larger than the scattered-field amplitudes and the CFI does not saturate the QCRB. Figures 2(b)–2(d) show the effect of the reference arm using MiSCAT. In Fig. 2(b) we consider the amplitude of $|\alpha_{\mathrm{i}}| = 4.5\times 10^{-5}|\alpha_0|$, which is large enough to saturate the QCRB for any phase ϕ_{s} of the scattered field, and show the relation between ϕ_{i} and ϕ_{s}. In this case of large enough amplitude $|\alpha_{\mathrm{i}}| \geqslant |\alpha_{\mathrm{r}} + \alpha_{\mathrm{s}}^{\mu}|$, we only adjust the phase of the reference arm, and the QFI is reached if $\cos(\psi - \chi) = 0$. In Fig. 2(c) we consider the parameters of the minimum CFI in Fig. 2(a), when $\phi_{\mathrm{s}} = 5\pi/6$ (blue dotted line). In Fig. 2(d) we consider CFI close to QFI by choosing $|\alpha_{\mathrm{r}}| = 0.01|\alpha_0|$. In both cases we show the ratio $F_{\mathrm{c}}^{m}/\mathscr{F}_{\mathrm{c}}^{m}$ as a function of $|\alpha_{\mathrm{i}}|$ and ϕ_{i}. If $|\alpha_{\mathrm{i}}|$ is lower than a certain value, we cannot reach the QCRB by changing ϕ_{i}. Thus, the total field amplitude is not large enough to touch the yellow dashed line in Fig. 1, which is the solution when $\psi = \chi$ for mass estimation. However, if $|\alpha_{\mathrm{i}}|$ is large enough to saturate the QFI, there are two solutions defined

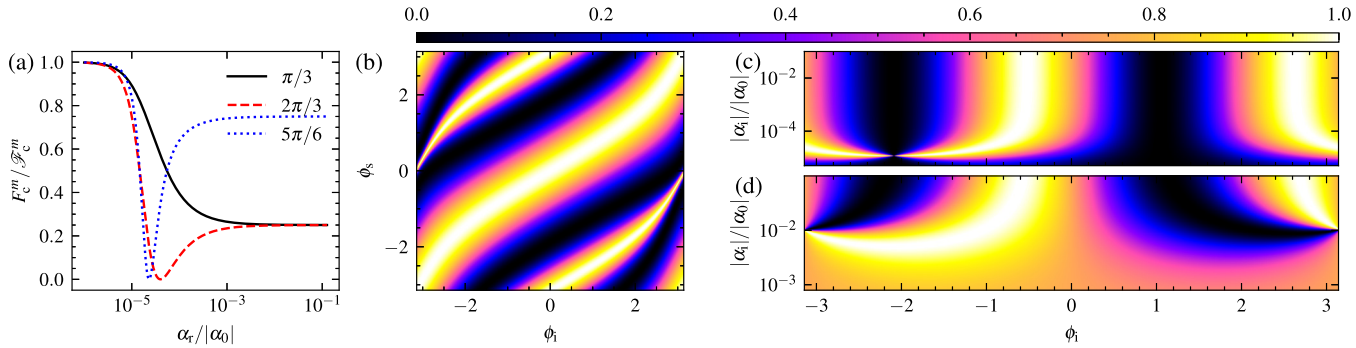

FIG. 2. Ratio $F_c^m/\mathscr{F}_c^m$ for coherent states as a function of different parameters considering mass estimation with a scattered-field amplitude $|\alpha_s| = 2 \times 10^{-5}|\alpha_0|$. (a) Plot of $F_c^m/\mathscr{F}_c^m$ as a function of α_r in logarithmic scale for the iSCAT considering different phases of the scattered field $\phi_s \in \{\pi/3, 2\pi/3, 5\pi/6\}$. (b) Density plot of $F_c^m/\mathscr{F}_c^m$ as a function of ϕ_s and ϕ_i using MiSCAT with $\alpha_r = 2.3 \times 10^{-5}|\alpha_0|$ and $\alpha_i = 4.5 \times 10^{-5}|\alpha_0|$. (c) and (d) Ratio $F_c^m/\mathscr{F}_c^m$ as a function of $|\alpha_i|$ and ϕ_i with $\phi_s = 5\pi/6$ using MiSCAT with (c) $\alpha_r = 2.3 \times 10^{-5}|\alpha_0|$ near the value for minimal CFI and (d) $\alpha_r = 10^{-2}|\alpha_0|$.

by two different phases ϕ_i. This implies that a variation of the phase ϕ_i for a large enough α_i allows one to saturate the QCRB with the intensity measurement. The intersection points in Figs. 2(c) and 2(d) correspond to a vanishing field $\alpha_d(\mu; \alpha_i, \phi_i) = 0$, i.e., a vacuum state. Thus, the CFI is not defined at this point since the vacuum has no defined phase. When the phase shift due to the particle is $\phi_s = \pi/2$, the CFI and signal-to-noise ratio (SNR) for iSCAT become extremely small for mass estimation [see Eq. (B2)]. This implies that the mean value of the probability distribution after the intensity measurement does not change with respect to the parameter m. In Appendix C we consider this case and compare it to MiSCAT with optimal phase ϕ_i and amplitude α_i. Then the mean value of the optimal probability distribution including the second arm becomes sensitive to the parameter m. This is corroborated by the SNR for mass estimation, which can be maximized by correctly tuning the phase ϕ_i of the second arm of the interferometer.

B. Saturating the QFI for phase estimation

One may also be interested in estimating the phase of the scattered field. Estimation of phase can contain additional information, e.g., in a wide-field iSCAT setup, the phase is related to the position of the particle [24]. There is a $\pi/2$ difference between optimally estimating ϕ_s and m, which arises from an additional factor i in the derivative of α_s^μ with respect to ϕ_s in Eq. (11). In Fig. 3(a) we show the ratio $F_c^{\phi_s}/\mathscr{F}_c^{\phi_s}$ as a function of α_r without the reference arm of the interferometer. Increasing α_r increases $F_c^{\phi_s}/\mathscr{F}_c^{\phi_s}$, which is a behavior opposite to the one for mass estimation. If $\alpha_r = 0$, the intensity measurement does not contain any phase information about α_s [31]. Thus, the existence of a relative phase and hence its measurability hinges on a nonvanishing value of α_r. However, to saturate the QCRB requires an $|\alpha_i|$ larger than $|\alpha_r + \alpha_s^\mu|$. We see in Fig. 3(b) for a small $\alpha_r = 0.01|\alpha_0|$ that we can saturate the QFI $\mathscr{F}_c^{\phi_s}$ of a coherent state for the phase estimation as well, if α_i is large enough and the phase ϕ_i is correctly tuned. Like for the estimation of the mass of the particle, we consider the relation between the SNR in both cases, for iSCAT and MiSCAT, as $\phi_s \to 0$. We see [see Eq. (B8)] that the SNR scales quadratically $\sim \phi_s^2$ for iSCAT and linearly $\sim \phi_s$ for MiSCAT for estimating ϕ_s. Thus, one can optimize the SNR by adjusting the phase ϕ_i of the second arm and achieve a better estimation of the phase shift due to the particle when it is very small.

In the case of a multifrequency coherent state, we can replace the Poisson probability distribution with a probability density for each frequency. Since we do not have any correlation between different frequency modes, the CFI for multifrequency coherent state in Eq. (18) generalizes to

$$F_f^\mu = 4 \int_{\Delta\omega} d\omega \left|\partial_\mu \alpha_s^\mu(\omega)\right|^2 \cos^2[\psi(\omega) - \chi(\omega)]. \quad (19)$$

Considering $F_f^\mu = \mathscr{F}_{pf}^\mu$, the QFI $\mathscr{F}_f^\mu$ for the multifrequency coherent state is an upper bound for both the CFI F_f^μ for multifrequency photon-number measurement on coherent states and the QFI $\mathscr{F}_{pf}^\mu$ for multifrequency phase-averaged states. The saturation of the $\mathscr{F}_f^\mu$ highly depends on the correct phase of the total field. In the experiment, if one cannot eliminate the reflected field, it is necessary to adjust the total phases of the field $\chi(\omega)$ of the detection modes using the reference

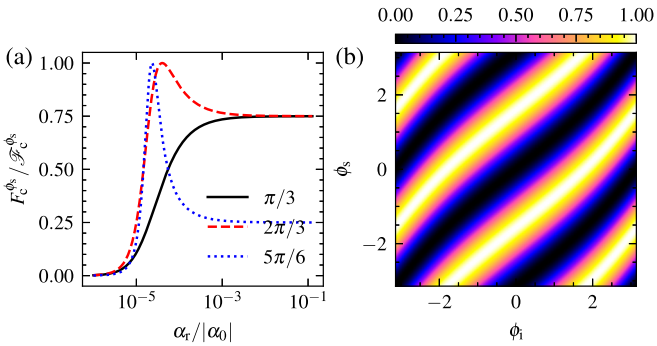

FIG. 3. Ratio $F_c^{\phi_s}/\mathscr{F}_c^{\phi_s}$ for coherent states as a function of different parameters considering phase estimation with the scattered field $|\alpha_s| = 2 \times 10^{-5}|\alpha_0|$. (a) Ratio $F_c^{\phi_s}/\mathscr{F}_c^{\phi_s}$ as a function of $|\alpha_r|$ in logarithmic scale for the iSCAT considering different phases of the scattered field $\phi_s \in \{\pi/3, 2\pi/3, 5\pi/6\}$. (b) Density plot of the ratio $F_c^{\phi_s}/\mathscr{F}_c^{\phi_s}$ as a function of ϕ_s and ϕ_i using MiSCAT with $\alpha_r = 0.01|\alpha_0|$ and $\alpha_i = 0.045|\alpha_0|$.

arm of the interferometer to match with the phase $\psi(\omega)$ of the derivative for each frequency component with respect to the parameter to be estimated.

IV. CONCLUSION

In this work we proposed a setup for optical photometry based on Rayleigh light scattering by integrating a Michelson interferometer into the conventional iSCAT microscope. We showed that precise control over the phase and amplitude of the reference field allows us to significantly enhance the estimation of both the mass and phase of nanoparticles. Our theoretical analysis, based on the classical Cramér-Rao bound (CRB) and QCRB, has rigorously established that MiSCAT outperforms conventional iSCAT by achieving optimal sensitivity for different quantum states, including single-mode coherent states, multifrequency coherent states, and phase-averaged coherent states. If the phase and amplitude of the reference field are optimally adjusted, the classical CRB using photon-number measurement saturates the QCRB using MiSCAT for estimating both the mass of the particle and the phase shift due to the particle. The ability to accurately measure the mass and phase of nanoparticles at the quantum limit of sensitivity has direct applications in single-molecule detection. By achieving the quantum limit of sensitivity, MiSCAT can be used in a number of different fields, including biophysics, molecular biology, and nanotechnology. While our study establishes the theoretical framework and fundamental advantages of MiSCAT, several experimental considerations remain to be addressed to fully take advantage of the enhanced sensitivity in real-world applications.

ACKNOWLEDGMENT

We thank Anita Jannasch and Viktor Schiff for invaluable insights and discussions, which significantly enriched this work.

APPENDIX A: QUANTUM CRAMÉR RAO BOUND AND QUANTUM FISHER INFORMATION FOR COHERENT STATES

For a given quantum state, the QFI is given by

$$\mathscr{F}^{\mu} = \mathrm{Tr}(\rho \mathscr{L}^2), \tag{A1}$$

where $\mathscr{L}$ is the symmetric logarithmic derivative of ρ_μ defined as

$$\rho_\mu \mathscr{L} + \mathscr{L}\rho_\mu = 2\partial_\mu \rho_\mu. \tag{A2}$$

In the case of coherent states the QFI becomes

$$\mathscr{F}_c^{\mu} = 4\sum_k (\langle \partial_\mu \alpha_k | \partial_\mu \alpha_k \rangle - |\langle \partial_\mu \alpha_k | \alpha_k \rangle|^2). \tag{A3}$$

In the Fock basis we can write

$$|\alpha_k\rangle = e^{-|\alpha_k|^2/2} \sum_{n=0}^{\infty} \frac{\alpha_k^n}{(n!)^{1/2}} |n\rangle_k. \tag{A4}$$

Calculating the first and second terms in the QFI using the orthonormality of Fock states, we have

$$\begin{aligned}\langle \partial_\mu \alpha_k | \partial_\mu \alpha_k \rangle = |\partial_\mu \alpha_k|^2 \Bigg(& |\alpha_k|^2 e^{-|\alpha_k|^2} \sum_{n=0}^{\infty} \frac{|\alpha_k|^{2n}}{n!} - |\alpha_k| \alpha_k e^{-|\alpha_k|^2} \sum_{n=1}^{\infty} \frac{|\alpha_k|^{2(n-1)}}{(n-1)!} - |\alpha_k| \alpha_k^* e^{-|\alpha_k|^2} \sum_{n=1}^{\infty} \frac{|\alpha_k|^{2(n-1)}}{(n-1)!} \\ & + e^{-|\alpha_k|^2} \sum_{n=1}^{\infty} \frac{n|\alpha_k|^{2(n-1)}}{(n-1)!} \Bigg),\end{aligned} \tag{A5}$$

$$\langle \partial_\mu \alpha_k | \alpha_k \rangle = \partial_\mu \alpha_k^* \left(-|\alpha_k| e^{-|\alpha_k|^2} \sum_{n=0}^{\infty} \frac{|\alpha_k|^{2n}}{n!} + \alpha_k e^{-|\alpha_k|^2} \sum_{n=1}^{\infty} \frac{|\alpha_k|^{2(n-1)}}{(n-1)!} \right). \tag{A6}$$

Using the following properties of the exponential series $\sum_{n=0}^{\infty} \frac{|\alpha_k|^{2n}}{n!} = e^{|\alpha_k|^2}$ and $\sum_{n=0}^{\infty} \frac{(n+1)|\alpha_k|^{2n}}{n!} = (1+|\alpha_k|^2)e^{|\alpha_k|^2}$, we can simplify

$$\begin{aligned}\langle \partial_\mu \alpha_k | \partial_\mu \alpha_k \rangle &= |\partial_\mu \alpha_k|^2 (2|\alpha_k|^2 - |\alpha_k|\alpha_k - |\alpha_k|\alpha_k^* + 1), \\ |\langle \partial_\mu \alpha_k | \alpha_k \rangle|^2 &= |\partial_\mu \alpha_k|^2 (2|\alpha_k|^2 - |\alpha_k|\alpha_k - |\alpha_k|\alpha_k^*).\end{aligned} \tag{A7}$$

Finally, the QFI [13] for the multimode coherent state becomes

$$\mathscr{F}_c^{\mu} = 4\sum_{k=1} |\partial_\mu \alpha_k|^2. \tag{A8}$$

We give the general formula for a multimode coherent state considering single-parameter estimation. In the case of a single mode with amplitude $\alpha_\mathrm{d} = \alpha_\mathrm{r} + \alpha_\mathrm{s}^\mu + \alpha_\mathrm{i}$ on the detector, we can find the QFI $\mathscr{F}_c^{\mu} = 4|\partial_\mu \alpha_\mathrm{s}^\mu|^2$.

APPENDIX B: SIGNAL-TO-NOISE RATIO

While the most fundamental analysis of the sensitivity of any measurement device is based on the QFI and QCRB, similar conclusions of how MiSCAT improves the sensitivity compared to iSCAT can be drawn from a simple analysis of the signal-to-noise ratio. We have a Poisson distribution of the photon number after the intensity measurement with a mean value given by the intensity of the total field I_d at the detector. We define the signal as the change in the mean I_d with respect to the parameter of interest μ as $\mu \frac{\partial I_\mathrm{d}}{\partial \mu}$. The noise is represented by the standard deviation due to shot noise, given by $\sqrt{I_\mathrm{d}}$. We begin with the iSCAT setup, considering the electric field at

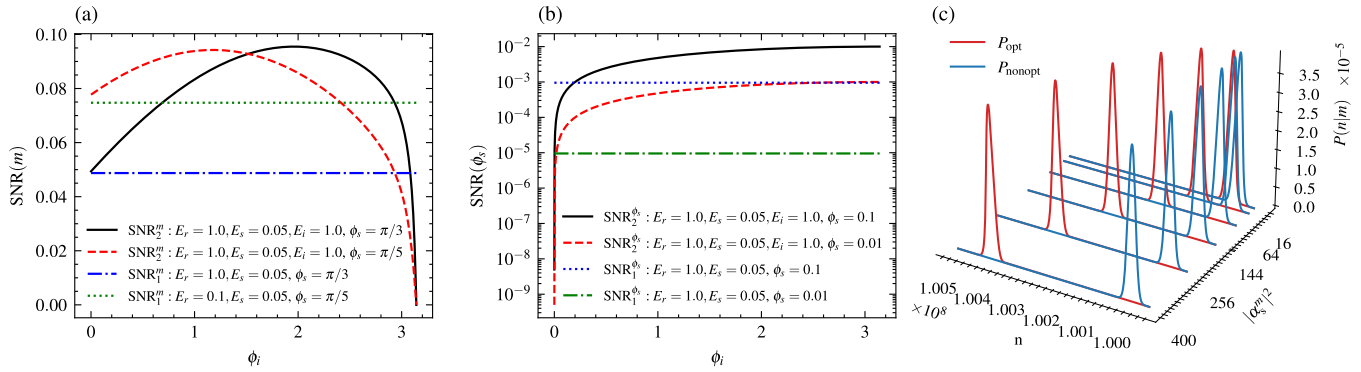

FIG. 4. (a) Plot of SNR(m) as a function of ϕ_i for estimating mass for different parameters. (b) Plot of SNR(ϕ_s) in logarithmic scale as a function of ϕ_i estimating phase shift due to the particle. (c) Photon-number distribution $P(n|\mu = m)$ as a function of $|\alpha_s^m|^2$ for optimized (red) and nonoptimized (blue) probability distributions to estimate mass.

the detector without the second arm. The electric field at the detector can be expressed as $E_d = E_r + E_s e^{i\phi_s}$, leading to the intensity

$$I_d^{(1)} = E_r^2 + 2E_r E_s \cos(\phi_s) + E_s^2. \tag{B1}$$

The mass m linearly scales with E_s and it gives the signal $2E_r E_s \cos(\phi_s)$ and $E_s \ll E_r$. Thus, the SNR [24] becomes

$$\mathrm{SNR}_1(m) = \frac{2E_r E_s \cos(\phi_s)}{\sqrt{E_r^2 + 2E_r E_s \cos(\phi_s) + E_s^2}}. \tag{B2}$$

We are also interested in the parameter ϕ_s. To understand the SNR around $\phi_s \sim 0$, we can expand the cosine terms up to the second order, $\cos(\phi_s) \approx 1 - \frac{\phi_s^2}{2}$, and find

$$I_d^{(1)} \approx E_r^2 - E_r E_s \phi_s^2 + 2E_r E_s + E_s^2. \tag{B3}$$

We observe that the first term involving ϕ_s is quadratic. Therefore, we can consider the signal related to the parameter as $2\phi_s^2 E_r E_s$, which scales proportionally to ϕ_s^2. Consequently, the SNR for iSCAT can be expressed for small values of ϕ_s as

$$\mathrm{SNR}_1(\phi_s) = \frac{2\phi_s^2 E_r E_s}{\sqrt{E_r^2 + 2E_r E_s + E_s^2}}. \tag{B4}$$

Let us now include the second arm of the interferometer as proposed in the main text for MiSCAT. Considering the total electric field at the detector as $E_d = E_r + E_s e^{i\phi_s} + E_i e^{i\phi_i}$, we can find the total intensity as

$$\begin{aligned} I_d^{(2)} &= E_i^2 + 2E_i E_r \cos(\phi_i) + 2E_i E_s \cos(\phi_i - \phi_s) \\ &\quad + E_r^2 + 2E_r E_s \cos(\phi_s) + E_s^2. \end{aligned} \tag{B5}$$

We have two terms that are linear in E_s, which translate into the signal used to analyze mass. Therefore, we can express the SNR for MiSCAT, including the second arm, as

$$\mathrm{SNR}_2(m) = \frac{2E_r E_s \cos(\phi_s) + 2E_i E_s \cos(\phi_i - \phi_s)}{\sqrt{E_i^2 + 2E_i E_r \cos(\phi_i) + 2E_i E_s \cos(\phi_i - \phi_s) + E_r^2 + 2E_r E_s \cos(\phi_s) + E_s^2}}. \tag{B6}$$

In the case of estimating a small phase shift $\phi_s \sim 0$, we have, by expanding the cosine term up to first order,

$$\begin{aligned} I_d^{(2)} &\approx E_i^2 + 2E_i E_r \cos(\phi_i) + 2E_i E_s \phi_s \sin(\phi_i) \\ &\quad + 2E_i E_s \cos(\phi_i) + E_r^2 + 2E_r E_s + E_s^2. \end{aligned} \tag{B7}$$

The signal is given by the term $2E_i E_s \phi_s \sin(\phi_i)$, while the remaining terms contribute to the noise. By assuming $E_s \ll E_r$ and keeping only the first-order term in E_s, we can express the signal-to-noise ratio as

$$\mathrm{SNR}_2(\phi_s) = \frac{2E_i E_s \phi_s \sin(\phi_i)}{\sqrt{E_i^2 + 2E_i E_r \cos(\phi_i) + E_r^2}}. \tag{B8}$$

In Fig. 4(a) we show the SNR as a function of ϕ_i for a signal used to analyze mass. It is clear that better performance is achieved when optimizing the second arm of the interferometer, compared to the conventional iSCAT setup. Furthermore, Fig. 4(b) confirms that accurate phase estimation for small particles is possible with the second arm. In both cases, these results are consistent with our calculations of the CRB.

APPENDIX C: MEASUREMENT TO ESTIMATE MASS

In iSCAT experiments, the standard detection methods are either cameras or photodiodes, both of which record intensity. For photon-number measurements, the positive-operator-valued measure is represented as $\Pi_n = |n\rangle\langle n|$, which corresponds to the intensity measurement in the case of single-mode coherent states and results in a Poisson probability distribution given by

$$P(n|\mu) = e^{-|\alpha_d|^2} \frac{|\alpha_d|^{2n}}{n!}, \tag{C1}$$

where $|\alpha_d|^2$ is the mean number of photons at the detector. As given in the main text, we have $\alpha_d = \alpha_r + \alpha_s^m + \alpha_i$ for MiSCAT, and we consider $\alpha_s^m = mse^{i\phi_s}$ as the field scattered from the particle, which carries the information about the mass m and the phase ϕ_s of the particle. In this case, we are interested in estimating mass and we set $\mu = m$. Usually $|\alpha_d|^2$ is very large for a typical setup. We can approximate the Poisson probability distribution by a Gaussian probability distribution using the well-known Stirling formula to get

$$P(n|\mu = m) \approx \frac{\exp\left(\frac{-[n-(|\alpha_d|^2-\frac{1}{2})]^2}{2|\alpha_d|^2}\right)}{|\alpha_d|\sqrt{2\pi}}. \tag{C2}$$

In Fig. 4(c) we show the probability distribution as a function of n and $|\alpha_s^m|^2$. When $\phi_s = \pi/2$, the SNR for iSCAT is extremely small. Then we include the second arm of the interferometer by setting $|\alpha_r| = |\alpha_i|$ and optimizing $P(n|\mu = m)$ over ϕ_i to estimate the mass using MiSCAT. One can see that the mean value of the probability distribution using MiSCAT, in red, is optimized to saturate the QFI for mass estimation changes when one changes $|\alpha_s^m|^2$. However, it remains constant for a nonoptimized probability distribution using iSCAT, in blue, which means that for $\phi_s = \pi/2$ one cannot estimate the mass with iSCAT.

[1] R. W. Taylor, R. G. Mahmoodabadi, V. Rauschenberger, A. Giessl, A. Schambony, and V. Sandoghdar, Nat. Photon. **13**, 480 (2019).

[2] R. W. Taylor and V. Sandoghdar, Nano Lett. **19**, 4827 (2019).

[3] G. Young, N. Hundt, D. Cole, A. Fineberg, J. Andrecka, A. Tyler, A. Olerinyova, A. Ansari, E. G. Marklund, M. P. Collier *et al.*, Science **360**, 423 (2018).

[4] J. Becker, J. S. Peters, I. Crooks, S. Helmi, M. Synakewicz, B. Schuler, and P. Kukura, ACS Photonics **10**, 2699 (2023).

[5] M. Dahmardeh, H. Mirzaalian Dastjerdi, H. Mazal, H. Köstler, and V. Sandoghdar, Nat. Methods **20**, 442 (2023).

[6] M. Piliarik and V. Sandoghdar, Nat. Commun. **5**, 4495 (2014).

[7] M. Tsang, R. Nair, and X.-M. Lu, Phys. Rev. X **6**, 031033 (2016).

[8] M. Tsang, Phys. Rev. A **99**, 012305 (2019).

[9] E. Köse, G. Adesso, and D. Braun, Phys. Rev. A **106**, 012601 (2022).

[10] E. Köse and D. Braun, Phys. Rev. A **107**, 032607 (2023).

[11] C. Lupo and S. Pirandola, Phys. Rev. Lett. **117**, 190802 (2016).

[12] C. W. Helstrom, J. Stat. Phys. **1**, 231 (1969).

[13] D. Bouchet, S. Rotter, and A. P. Mosk, Nat. Phys. **17**, 564 (2021).

[14] D. Bouchet, J. Dong, D. Maestre, and T. Juffmann, Phys. Rev. Appl. **15**, 024047 (2021).

[15] Y. Shechtman, S. J. Sahl, A. S. Backer, and W. E. Moerner, Phys. Rev. Lett. **113**, 133902 (2014).

[16] S. L. Braunstein and C. M. Caves, Phys. Rev. Lett. **72**, 3439 (1994).

[17] L. Priest, J. S. Peters, and P. Kukura, Chem. Rev. **121**, 11937 (2021).

[18] S. Lin, Y. He, H. M. L. Robert, H. Li, P. Zhang, M. Piliarik, and X.-W. Chen, J. Phys. D **54**, 274002 (2021).

[19] R. Gholami Mahmoodabadi, R. W. Taylor, M. Kaller, S. Spindler, M. Mazaheri, K. Kasaian, and V. Sandoghdar, Opt. Express **28**, 25969 (2020).

[20] A. P. Vinogradov, V. Y. Shishkov, I. V. Doronin, E. S. Andrianov, A. A. Pukhov, and A. A. Lisyansky, Opt. Express **29**, 2501 (2021).

[21] D. S. Bradshaw, K. A. Forbes, and D. L. Andrews, Eur. J. Phys. **41**, 025406 (2020).

[22] C. F. Bohren and D. R. Huffman, *Absorption and Scattering of Light by Small Particles*, 1st ed. (Wiley, New York, 1998).

[23] A. Weigel, A. Sebesta, and P. Kukura, ACS Photonics **1**, 848 (2014).

[24] J. Dong, D. Maestre, C. Conrad-Billroth, and T. Juffmann, J. Phys. D **54**, 394002 (2021).

[25] A. V. Failla, S. Jäger, T. Züchner, M. Steiner, and A. J. Meixner, Opt. Express **15**, 8532 (2007).

[26] A. V. Failla, H. Qian, H. Qian, A. Hartschuh, and A. J. Meixner, Nano Lett. **6**, 1374 (2006).

[27] H. M. Dastjerdi, M. Dahmardeh, A. Gemeinhardt, R. Gholami Mahmoodabadi, H. Köstler, and V. Sandoghdar, J. Phys. D **55**, 054002 (2022).

[28] G. Young and P. Kukura, Annu. Rev. Phys. Chem. **70**, 301 (2019).

[29] M. Küppers, D. Albrecht, A. D. Kashkanova, J. Lühr, and V. Sandoghdar, Nat. Commun. **14**, 1962 (2023).

[30] K. Lindfors, T. Kalkbrenner, P. Stoller, and V. Sandoghdar, Phys. Rev. Lett. **93**, 037401 (2004).

[31] O. Hauler, F. Wackenhut, L. A. Jakob, A. Stuhl, F. Laible, M. Fleischer, A. J. Meixner, and K. Braun, Nanoscale **12**, 1083 (2020).

[32] O. Hauler, L. A. Jakob, K. Braun, F. Laible, M. Fleischer, A. J. Meixner, and F. Wackenhut, J. Phys. Chem. C **125**, 6486 (2021).

[33] F. Wackenhut, L. A. Jakob, O. Hauler, A. Stuhl, F. Laible, M. Fleischer, K. Braun, and A. J. Meixner, Anal. Bioanal. Chem. **412**, 3405 (2020).

[34] R. J. Glauber, Phys. Rev. **131**, 2766 (1963).

[35] A. Allevi, M. Bondani, P. Marian, T. A. Marian, and S. Olivares, J. Opt. Soc. Am. B **30**, 2621 (2013).

[36] L. Mandel and E. Wolf, *Optical Coherence and Quantum Optics*, 1st ed. (Cambridge University Press, Cambridge, 1995).

[37] A. Stollmann, J. Garcia-Guirado, J.-S. Hong, P. Rüedi, H. Im, H. Lee, J. Ortega Arroyo, and R. Quidant, Nat. Commun. **15**, 4109 (2024).